Progress In Electromagnetics Research, Vol. 166, 59–74, 2019

Filter-Free Light Absorption Measurement of Volcanic Ashes and Ambient Particulate Matter Using Multi-Wavelength Photoacoustic Spectroscopy

Gaoxuan Wang[1], Pierre Kulinski[1], Patrice Hubert[2], Alexandre Deguine[2], Denis Petitprez[2], Suzanne Crumeyrolle[3], Eric Fertein[1], Karine Deboudt[1], Pascal Flament[1], Markus W. Sigrist[4], Hongming Yi[1#], and Weidong Chen[1, *]

Abstract—Accurate measurement of atmospheric particulate matter (PM) absorption coefficient is highly required for study of earth climate change and for monitoring of air quality. In addition, multi-wavelength measurements of PM absorption can provide information on the PM chemical composition (black carbon or brown carbon). A multi-wavelengths photoacoustic (MW-PA) spectrophone operating at 444, 532 and 660 nm was developed and deployed for filter-free characterization of wavelength-dependent optical properties of PM mass absorption coefficient (MAC) and absorption Ångström coefficient (AAC). It is worth noting that to date no any AAC of volcanic ashes determined by filter-free measurement have been reported. The developed MW-PA spectrophone was deployed to an intensive field campaign measurement of environmental PM in Grenoble (France). Side-by-side inter-comparison measurements of ambient PM showed a good correlation between the developed MW-PA spectrophone and a reference instrument aethalometer (Magee scientific, AE33).

1. INTRODUCTION

Atmospheric particulate matter (PM), emitted by anthropogenic and natural sources, strongly affects the radiative budget of the earth's atmosphere through scattering or absorbing the solar radiation, which provides negative (cooling) or positive (warming) radiative forcing (RF) effects on the earth climate [1]. The PM radiative forcing strongly depends on its optical depth (AOD) and light absorption [2]. However, PM light absorption used for prediction of earth's future climate is known with large uncertainties due to the lack of appropriate instrumentation for high-precision measurements [3–6]. In addition, PM in air is also an important pollutant and is considered as the most significant environmental issue on public health, which causes respiratory diseases, cardiovascular diseases and epidemic [7, 8]. Air pollution level is characterized by its mass concentration that is deduced from its light absorption coefficient divided by its mass absorption coefficient (MAC) [9]. Therefore, accurate measurement of PM's light absorption coefficient is highly required for both climate change study and air quality monitoring.

The commonly used method for the measurement of atmospheric PM absorption is based on filer-sampling of PM. PM is collected on a filter, and the light attenuation through the filter is measured to deduce the PM absorption coefficient [10]. This method suffers, however, from filter loading effect during the accumulative process of PM, which might overestimate the light absorption with an uncertainty of up to 20–30% [11, 12]. An alternative method widely used is "difference method", which derives from the

Received 6 October 2019, Accepted 12 October 2019, Scheduled 4 November 2019
* Corresponding author: Weidong Chen (chen@univ-littoral.fr).
[1] Laboratoire de Physicochimie de l'Atmosphère, Université du Littoral Côte d'Opale, Dunkerque, France. [2] Physicochimie des Processus de Combustion et de l'Atmosphère, Université de Lille 1, Villeneuve d'Ascq, France. [3] Laboratoire d'Optique Atmosphérique, Université de Lille 1, Villeneuve d'Ascq, France. [4] Laser Spectroscopy and Sensing Laboratory, Institute of Quantum Electronics, ETH Zurich, Switzerland. # now with Princeton University, USA.

difference between the measured light extinction and scattering coefficients of the PM to determine its absorption coefficient [7, 13]. This method exhibits significant uncertainty resulting from the subtraction of near-identical values of extinction and scattering coefficients [14].

Photoacoustic spectroscopy is commonly recognized as one of the best tools for filter-free direct measurement of PM absorption, with advantages of high accuracy, high portability for field measurements, and less sensitivity to scattering than filter-based method. Photoacoustic spectroscopy relies on the generation of acoustic sound by transferring intensity-modulated electromagnetic light energy into thermal energy [15, 16]. Light absorbed by suspending particles might heat the surrounding air. If the incident light is modulated, a thermal wave at the modulated frequency is generated. The thermal wave variation results in an acoustic signal. An acoustic resonator is usually used to amplify the acoustic signal that can be measured using microphone. The acoustic wave ($p(\mathbf{r}, t)$) within a resonator can be expressed by the following wave equation [17, 18]:

$$\partial_t^2 p(\tilde{\mathbf{r}}, t) - c_s^2 \nabla^2 p(\mathbf{r}, t) = (\eta - 1)\partial_t H(\mathbf{r}, t) \tag{1}$$

Eq. (1) establishes a mathematical model between acoustic wave $p(\mathbf{r}, t)$ and heat production $H(\mathbf{r}, t)$. It should be mentioned that all dissipative terms due to heat diffusion and dynamic viscosity are neglected in this equation [17]. The heat production $H(\mathbf{r}, t) = \sigma N P g(\mathbf{r}) e^{i\omega t}$ is induced by the optical energy deposited in the sample by light absorption. $g(\mathbf{r})$ is the normalized function for the spatial distribution of light intensity (its integral over the entire cross section of the light beam is equal to unity) [18]. N is the number concentration of the absorber, and σ is its absorption cross-section. P is the excitation light power. ω represents the angular-frequency of the light. c_s is the speed of sound in vacuum, and η is the ratio of specific heats of the gas for constant pressure and volume inside the acoustic resonator. The amplitude of the nth eigenmode acoustic component is expressed as follows [18]:

$$A_n = \frac{(\eta - 1) Q_n}{\omega_n} \frac{F_n \sigma N P L}{V_\mathrm{res}} \tag{2}$$

where ω_n is the angular frequency of the nth eigenmode component A_n; Q_n is the quality factor of the nth eigenmode component; $\mathrm{V_{res}}$ is the resonator volume. F_n describes the spatial overlap between the propagating light beam and the pressure distribution of the nth acoustic eigenmode. L is the resonator length. Eq. (2) derives the unique advantage of photoacoustic spectroscopy that its sensitivity is directly proportional to the optical excitation power.

Broadband measurements of PM absorption coefficients have been used to infer black carbon or brown carbon mass to identify ambient chemical composition [19]. Multi-wavelength photoacoustic (MW-PA) spectrophone is usually used for measuring wavelength-dependent PM absorption coefficients [20–25]. Light source as a key element in photoacoustic (PA) spectrophone directly determines the spectrophone performance via its light power and emission wavelength. Various light sources are used for MW-PA spectrophone applications, including: (1) broadband arc lamp or supercontinuum laser source. (2) multiple narrow-bandwidth diode lasers.

In MW-PA spectrophone using broadband light source, selection of working wavelength bands is generally achieved by using a series of bandpass filters [20, 21]. A broadband Hg arc lamp (Optical Building Blocks, LPS 100) was used by Wiegand et al. to realize a PA spectrophone operating at 8 discrete wavelengths in the spectral range of 300–700 nm [20]. The MW-PA spectrophone was capable of providing 186 (bandwidth of 7 nm) to 382 (bandwidth of 17 nm) mW of optical powers resulting in minimum detect limits of 2.6 and 1.3 $\mathrm{Mm^{-1}}$ (20 s integration time), respectively. Sharma et al. developed an MW-PA spectrophone at 5 discrete wavelengths in the range of 417–675 nm using a supercontinuum laser source (Fianium Inc. SC400) [21]. Typical optical powers were 45 mW with a bandwidth of 56 nm and 86 mW in a bandwidth of 80 nm. This photoacoustic spectrometer was validated by study of laboratory-generated particle of kerosene soot and salt with minimum detect limits of 0.5–4 $\mathrm{Mm^{-1}}$ (60 s). Selection of wavelength and bandwidth can be achieved using an optical filter wheel [20, 21] or tunable wavelength and bandwidth filter [22] that can provide 22 discrete wavelengths from 500 to 840 nm with wavelength resolutions of about 10–20 nm.

Diode lasers, owing to its high power density and narrow emission bandwidth, are widely used as light source in MW-PA spectrophone [23–25]. Lewis et al. developed a three-wavelength (405, 532, 781 nm) MW-PA spectrophone, commercialized as the PASS-3 (Droplet Measurement Technologies, Boulder, CO) [23]. Recently, Linke et al. developed an MW-PA spectrophone using three diode lasers

emitting at 445, 532, and 660 nm with light powers of 150, 100, and 50 mW, respectively [24]. It was used for laboratory study on soot and urban field measurement of ambient PM with detection limits of 5.6 (at 450 nm), 6.6 (at 532 nm), and 1.8 (at 660 nm) Mm^{-1}, respectively.

This paper reports a compact 3-wavelength PA spectrophone based on diode lasers operating at 444, 532, and 660 nm in a single PA resonator. Wavelength-dependent optical properties (mass absorption coefficient, MAC and absorption Ångström coefficient, AAC) of volcanic ashes sampled from 2010 eruptions of Eyjafjallajökull were characterized in laboratory. The potential ability of the MW-PA spectrophone for PM measurement in environmental conditions was demonstrated through an inter-comparison with a reference instrument aethalometer MAGEE AE33 in a field campaign.

2. EXPERIMENTAL SETUP

2.1. Development of a 3-Wavelength PA Spectrophone

Figure 1(a) describes the architecture of the developed 3-wavelength PA spectrophone. Three diode lasers emitting respectively at 444, 532, and 660 nm are used as light excitation sources. The three lasers are modulated, through a mechanical chopper, at the 1st longitudinal resonant frequency (6260 Hz) of the used PA resonator. The blue diode laser (NICHIA, NDB7875) emits at 444 nm with an output power of 1200 mW (powered with a diode current I_D = 1100 mA and V = 5.1 V using a diode laser controller Arryo instrument, 6340). The blue laser has typical divergence angels of 44° ($\theta_\perp$) at vertical direction and 14° ($\theta//$) at horizontal direction. A NA = 0.5 microscopy lens was used to collimate the light beam. The green laser module (Medialas, DPGL 750) operating at 532 nm has a collimated output beam with a diameter of 3 mm and an output power of 750 mW powered at 5 V. The red laser module (Medialas, ML101J27) emitting at 660 nm has an output power of 130 mW and is driven by a laser diode controller (Stanford, LDC 501) with a diode current of 200 mA.

A high quality dichroic filter D1 (Medialas, model dichro rot) is used to couple the red light (by reflection) and the green light (by transmission) to the PA cell (as shown in Fig. 1(a)). An optical filter D2 (Edmund) with a passband of 525–1075 nm (used to transmit the red and green lights) and a rejection of wavelengths less than 525 nm (used to couple the blue light by its reflection) are used to couple all three light beams to the PA cell. Lens f_1 with a local length of 10-mm and a diameter of 10 mm is used to reshape laser beams and focus them on a 100-slot mechanical chopper (used for light modulation). The modulated laser beams are then collimated by lens f_2 (with a local length of 10-mm and a diameter of 10 mm) and directed towards the PA cell. The modulated light powers behind the PA cell are 260 mW (444 nm), 180 mW (532 nm), and 35 mW (660 nm), respectively.

In the present work, a single acoustic resonator was used. Measurements of PA signal at each

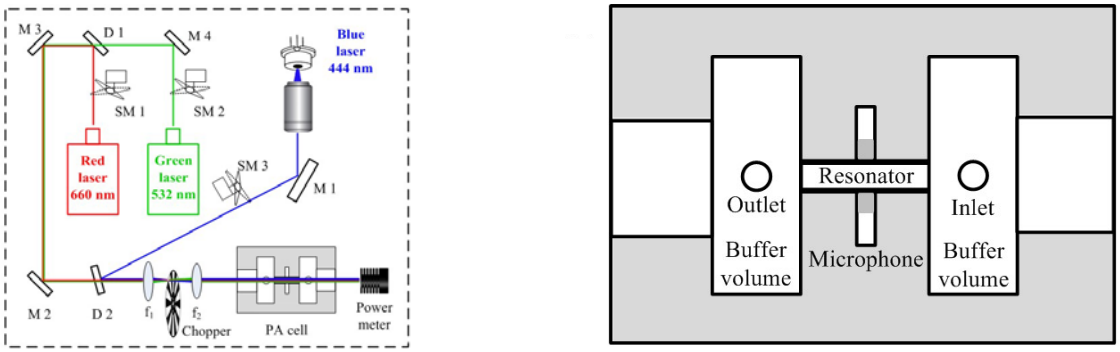

(a) (b)

Figure 1. (a) Schematic view of the 3-wavelength PA spectrophone. M1, M2, M3, M4: mirrors. f_1, f_2: lens. D1: dichroic filter. D2: shortpass optical filter (transmission wavelength: 525–1075 nm; rejection wavelength: 1210–1470 nm). SM1, SM2, SM3: servomotor. (b) Structure of the used longitudinally resonant PA cell.

wavelength are then separately performed. Three parallax standard servomotors (SM1, SM2, SM3) were used to let the selected light beam pass through the PA cell sequentially for the measurements. Position of the servo shaft is controlled by an Arduino microcontroller (Arduino, UNO Rev3).

Figure 1(b) shows a schematic drawing of our PA cell consisting of a resonator and two buffer volumes [26]. A single-pass longitudinally resonant cylinder is used as acoustic resonator with lengths of 23 mm and 6 mm in diameter, which gives the 1st longitudinal acoustic resonant frequency of 6260 Hz. Two buffer volumes at each extreme side of the PA cell can minimize the noise resulting from sample flow or light absorption from window [18]. The PA cell is sealed with UV fused silica windows that have high optical transmission of $> 90\%$ from 180 nm to 2.6 μm. Electret microphone (EK-23329-P07, Knowles) located at the middle of cylindrical resonator is used for detecting PA signal with a sensitivity of 22.4 mV/Pa at the sound frequency from 100 to 10000 Hz. A lock-in amplifier (Stanford, SR830) is adopted to demodulate the microphone signal at the light modulation frequency. A power meter (Coherent, LM 10) is used to record the light power to normalize acoustic signals. The PA signal is then sampled by a data digitalization card (National Instrument, model 6251), and a laptop is used to perform data processing and result display via a Labview interface.

2.2. Experimental Set-up for Volcanic Ash Measurements in Lab

Figure 2 shows the schematic diagram of the experimental setup used for determination of light absorption of volcanic ashes samples. The experimental setup contains a particle generation module, an MW-PA spectrophone, and an aerodynamic particle sizer (APS) (TSI, APS 3321) that can measure particle mass concentration in a size range of 0.5–20 μm. The particle generation module described in Fig. 2 includes a magnetic stirring hot plate (Heidolph, MR 3001K) for raising up volcanic ashes, a mass flow controller MFC1 (MFC, Bronkhorst, EL-FLOW) to control the flow rate of nitrogen used as carrier gas, and a laboratory flask used as a buffer chamber for uniformly mixing volcanic ashes.

After raised up by the magnetic stirring hot plate, the floating volcanic ashes were divided into two parts. One part was directed towards the PA spectrophone and the APS, and the other part is open for excess flow. The mass flow controller MFC2 was used to dilute the volcanic ashes concentration behind the laboratory flask using nitrogen at a flow rate of 1.4 L/min. After dilution, volcanic ashes were separated into two lines: one to the PA sensor at a flow rate of 0.3 L/min and the other to the APS at a flow rate of 1.3 L/min. The inlet of the PA cell was divided into two lines too: one line

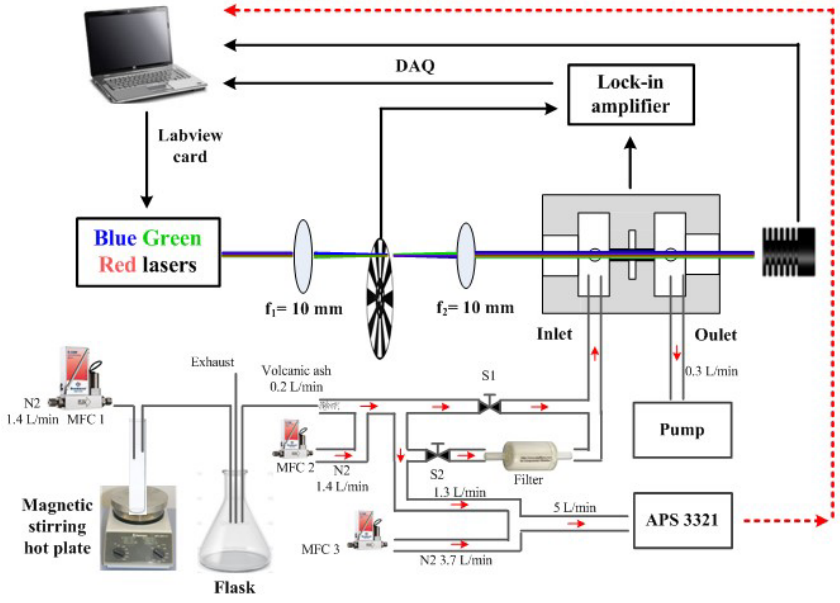

Figure 2. System schematic of the experimental setup for the measurements of volcanic ashes. S1, S2: valves. MFC1, MFC2, MFC3: mass flow controller. APS 3321: aerodynamic particle sizer.

contains a filter to remove residual particles for the measurement of background PA signal and the other without filter for injection of volcanic ashes to the PA cell. In this experiment, an N_2 flow rate of 3.7 L/min controlled by MFC3 and a flow rate of 1.3 L/min for volcanic ashes were combined to provide a flow rate of 5 L/min needed for the APS 3321 measurement. It should be noticed that volcanic ashes concentration measured by the APS is diluted by 3.85 times by such a mixture, and the real volcanic ashes concentration in the PA cell is 3.85 times the value inside the APS.

2.3. PA Spectrophone Integration for Field Campaign

For field deployment, all components of the 3-wavelength PA spectrophone including optical and electronic elements were integrated in a box as presented in Fig. 3(a) for installation in a minibus. The optical elements, such as diode lasers, optical lens, and PA cell, were installed on an optical table that was placed at the top of the box. The electronic elements including diode laser controllers, Arduino uno card, power supply, and two batteries were installed at the bottom of the box. Two fans were used to dissipate heats released from electronic elements, and a thermocouple was used to monitor the temperature in the box. Fig. 3(b) shows the box picture accompanied with a lock-in amplifier (Stanford Research Inc., SR830) for phase-sensitive detection of PA signal and a computer for recording, processing, and displaying the data.

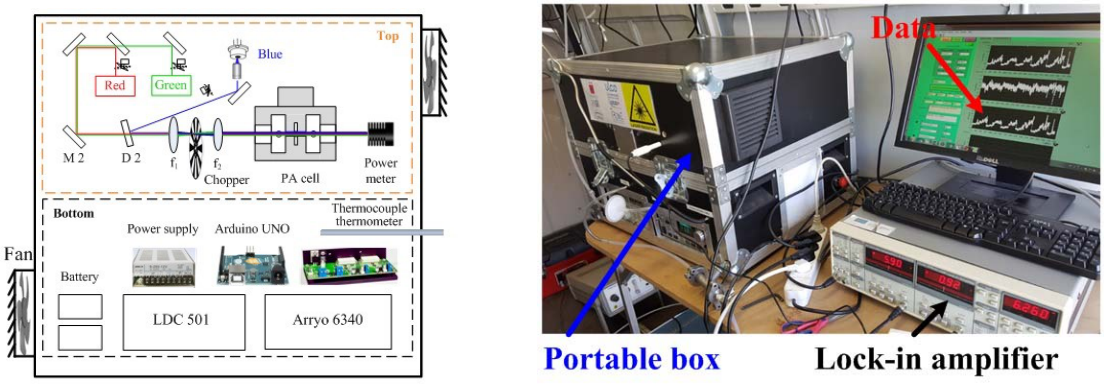

(a) (b)

Figure 3. (a) Integration of the developed 3-wavelength PA spectrophone in a compact box. (b) 3-wavelength PA spectrophone in a compact box associated with a compute and a lock in amplifier.

3. EXPERIMENTAL RESULTS AND DISCUSSION

3.1. PA Cell Calibration

The measured PA signal amplitude from the microphone depends on the used microphone sensitivity (M in [mV/Pa]), sample absorption coefficient (α_{abs} in [Mm^{-1}]), excitation light power (P in [W]), and PA cell constant ($C_{\text{cell}} = (\eta - 1)Q_n F_n L/\omega_n V_{\text{res}}$, in [Pa·m·W^{-1}]) that characterizes the conversion efficiency of thermal energy into acoustic energy in a PA cell. The PA signal, S_{PA} in [V], can be expressed as follows [18, 27]:

$$S_{\text{PA}} = M \times A_n + S_b = P \times M \times C_{\text{cell}} \times \alpha_0 \times C + S_b \tag{3}$$

where S_b, in [V], is the background PA signal that is generated by light absorbed on the walls or on the windows of the PA cell.

For PM measurement, α_0 is the PM mass absorption coefficient (MAC) in [m^2/g], which is expressed as α_{MAC} in the following section. C in [µg/m^3] is the PM mass concentration.

For trace gas measurement, α_0 is the specific gas absorption coefficient in [Mm^{-1}/ppbv], and C is the gas sample concentration in [ppbv].

As shown in Eq. (3), once the PA cell constant (C_{cell}) is known, the PM mass absorption coefficient (α_{MAC}) can be determined from the experimentally measured values S_{PA}, S_b, P and the PM mass concentration C. The PA cell constant (C_{cell}) can be calibrated with known absorption coefficient using Eq. (3). It should be noticed that the determination of PM mass absorption coefficient is based on the assumption that the cell constant (C_{cell}) is independent of the absorber being measured (gas or PM), and the adiabatic index η in air is the same [4, 28].

In this experiment, determination of the PA cell constant was performed using NO_2 absorption spectra at different NO_2 concentrations. NO_2 concentrations varying from 20 to 300 ppbv were generated from an Ansyco electronic charge device (KT-GPTM) through chemical reaction of NO (8 ppmv) with O_3 (that was produced by O_2 photolysis). The NO_2 concentrations were measured with a NOx analyzer (Thermal, Model 42i). The NO_2 specific absorption coefficient α_0 is determined by the following equation:

$$\alpha_0 = \frac{\sigma \times N}{C} \tag{4}$$

Given a NO_2 sample concentration of $C = 1$ ppbv, the corresponding NO_2 number concentrations $N = 2.49\times10^{14}$ molecule/cm^3 at $T = 293.5$ K and $P = 1$ atm and the absorption cross sections σ of 4.75×10^{-19} cm^2/molecule (at 444 nm), 1.52×10^{-19} cm^2/molecule (at 532 nm) and 7.57×10^{-21} cm^2/molecule (at 660 nm) [29], respectively, the specific absorption coefficient α_0 of NO_2 at 444, 532 and 660 nm were determined to be 1.18 Mm^{-1}/ppbv, 0.36 Mm^{-1}/ppbv, and 0.02 Mm^{-1}/ppbv.

Figure 4 shows different NO_2 concentrations measured by the NOx analyzer and the corresponding PA signals resulting from the blue, green, and red lasers, respectively. The PA signals from different laser excitations were acquired in sequence. The PA signals from the blue and green lasers increased linearly with NO_2 concentrations, while the PA signals induced by the red laser excitation remained almost constant regardless of NO_2 concentrations. It resulted from the weak red light power of only 35 mW (through the PA cell) and the weak NO_2 absorption at 660 nm (with an absorption cross-section of 7.57×10^{-21} cm^2/molecule) [29], in comparison to light powers of 265 mW at 444 nm and 185 mW at 532 nm, associated with a relatively higher absorption cross-sections (4.75×10^{-19} cm^2·mol^{-1} and 1.52×10^{-19} cm^2·mol^{-1} [29] for the blue and green lasers, respectively).

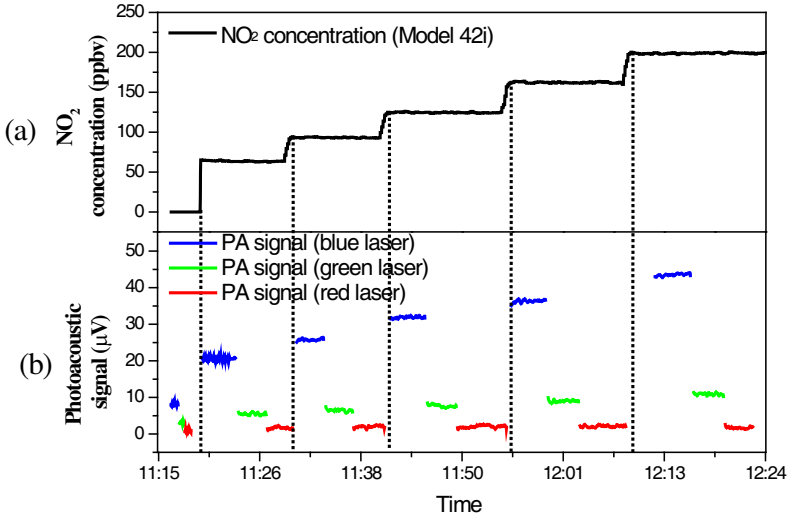

Figure 4. Time-series measurements using: (a) a NOx analyzer Model 42i for NO_2 concentration, and (b) the developed 3-wavelengths PA spectrophone for PA signals resulted from NO_2 absorptions.

Figure 5 plots the PA signals from the blue and green lasers vs. NO_2 concentrations. Two linear fits of the PA signals (y) to the NO_2 concentrations (x) are carried out: $y = 0.181x + 0.225$ for the blue laser, and $y = 0.038x - 0.120$ for the green laser, both with a regression coefficient $R = 0.998$. Based on

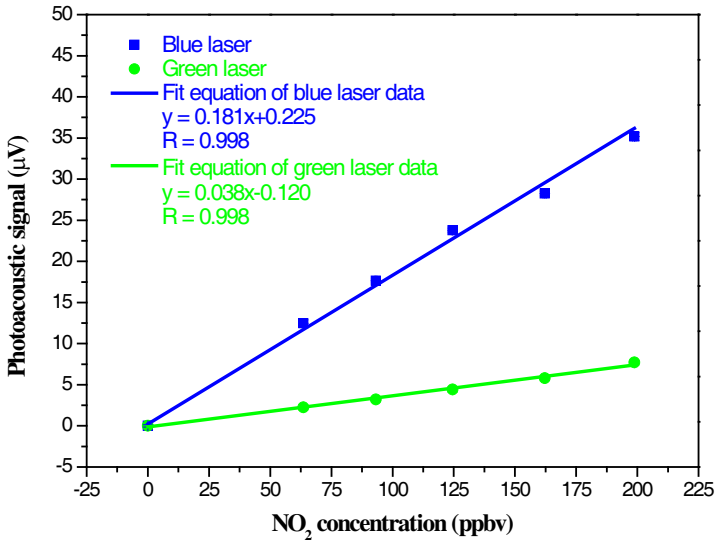

Figure 5. PA signals induced from the blue and the green lasers versus NO_2 concentrations.

the slopes S_{slope} of the linear fits (0.181 μV/ppbv and 0.038 μV/ppbv) and using the following equation:

$$C_{\text{cell}} = \frac{S_{\text{slope}}}{P \times M \times \alpha_0} \tag{5}$$

Cell constants C_{cell} of $6.58 \pm 0.21\,\text{Pa·m·W}^{-1}$ and $6.54 \pm 0.32\,\text{Pa·m·W}^{-1}$ for the blue and green laser are determined, respectively.

Uncertainty in the determined PA cell constant (ΔC_{cell}) is deduced from the uncertainties (ΔS_{EPA}) in the effective PA signal S_{EPA}($S_{\text{EPA}} = S_{\text{PA}} - S_{\text{b}}$), ΔC_{NO2} in the measured NO_2 concentration (C_{NO2}) using the NOx analyzer and ΔP in the laser power P and the uncertainties ($\Delta\alpha_0$) in the used cross section of NO_2 (3%) [29], as shown in Table 1. The uncertainty ΔC_{cell} in the calibrated cell constant C_{cell} is calculated by:

$$\frac{\Delta C_{\text{cell}}}{C_{\text{cell}}} = \sqrt{\left(\frac{\Delta S_{\text{EPA}}}{S_{\text{EPA}}}\right)^2 + \left(\frac{\Delta C_{\text{NO}_2}}{C_{\text{NO}_2}}\right)^2 + \left(\frac{\Delta P}{P}\right)^2 + \left(\frac{\Delta\alpha_0}{\alpha_0}\right)^2} \tag{6}$$

Table 1. Relative measurement uncertainties in the PA signal S_{EPA}, in the fluctuation of NO_2 concentration C_{NO2}, in the laser power P and in the NO_2 specific absorption coefficient α_0.

Diode laser	$\Delta S_{\text{EPA}}/S_{\text{EPA}}$ (%)	$\Delta P/P$(%)	$\Delta C_{\text{NO2}}/C_{\text{NO2}}$ (%)	$\Delta\alpha_0/\alpha_0$ (%)
444 nm	1.1	0.1	0.5	3.0
532 nm	3.9	0.2		

The relative uncertainties in the determined cell constants C_{cell} are 3.2% for blue laser and 4.9% for green laser, respectively. Finally, an averaged cell constant of $6.56 \pm 0.27\,\text{Pa·m·W}^{-1}$ (with an averaged uncertainty of 4.1%) is used in the following measurement as it is assumed to be wavelength-independent. With the calibrated cell constant and the known PM concentration, the wavelength-dependent mass absorption coefficient can be measured using the developed 3-wavelength PA spectrophone.

3.2. Laboratory Measurements of Volcanic Ash

Volcanic ashes are an important source of PM to the atmosphere. Volcano eruptions introduce high variability to the total global particulates burden [30]. Deposit of volcanic ashes on the surface of

glaciers drastically affect the physical and optical properties of snow and ice which accelerates the melt of glacier [31]. Volcanic ashes have the potential to influence the earth's radiation balance and pose hazards to human health [32]. Accurate knowledges of volcanic ashes' composition and optical absorption coefficient are needed for precise evaluation of their effects.

Measurement of light absorption of volcanic ashes at 444, 532, and 660 nm was performed using the developed 3-wavelength PA spectrophone. Two samples (A and B) of volcanic ashes were investigated in the present work. The volcanic ashes samples were collected from the volcano Eyjafjallajökull at the south of Iceland at different sample sites, provided by the laboratory of service de Chimie quantique et Photophysique (CQP), Université Libre de Bruxelles.

After the calibration of the 3-wavelength PA spectrophone with NO_2, volcanic ash measurements were performed. A complete measurement cycle included ~20 min sample measurement and ~15 min background measurement. The PA signals at 444, 532, and 660 nm were sequentially recorded at the sampling period. For background signal measurements, volcanic ashes were removed using a filter by switching valve S1 off and S2 on (Fig. 2). The background PA signals at 444, 532, and 660 nm were sequentially recorded with nitrogen injecting into the PA cell. The PA signals induced by the light absorption of volcanic ash were achieved by subtracting the background PA signals (grey area in Fig. 6) from the measured PA signals resulting from the samples (light blue area in Fig. 6). Fig. 6 shows the recorded PA signals vs. the corresponding volcanic ash mass concentrations measured with an aerodynamic particle sizer. The volcanic ash mass concentrations and PA signals within the sampling period were averaged for data analysis. The standard deviations in the measured volcanic ash mass concentrations and PA signals were used to estimate the measurement uncertainty. In the present work, the main uncertainty in the measurements of volcanic ashes' optical properties using the developed 3-wavelength PA spectrophone resulted from the fluctuation in the lab-generated volcanic ash mass concentrations.

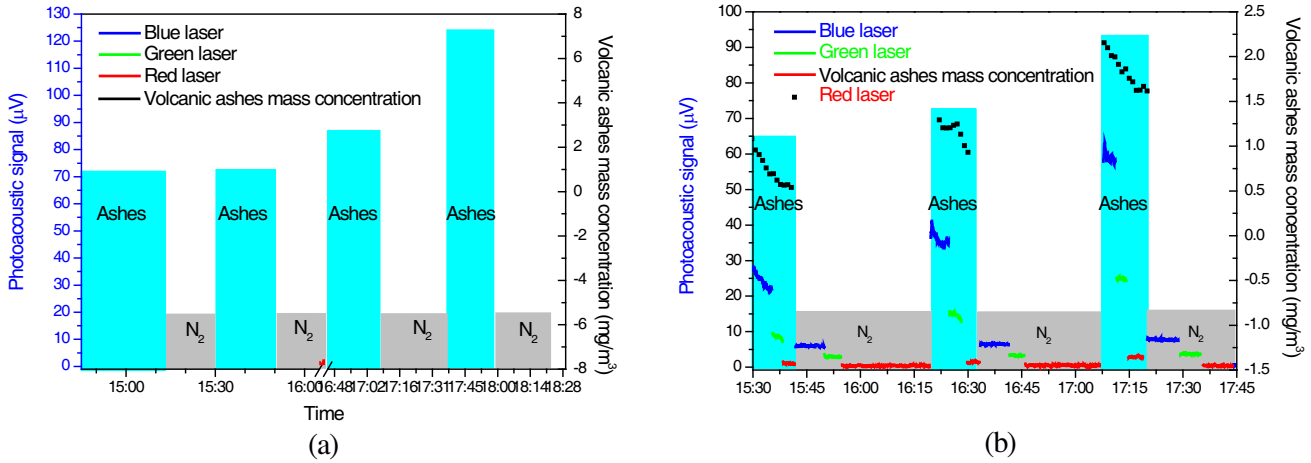

Figure 6. Time series measurements of PA signal following the variation in volcanic ash concentrations of (a) sample A and (b) sample B with 1 s integration time.

It is worth noting that the red laser power (35 mW) was not powerful enough for the measurement of volcanic ashes at low concentration, and relatively high concentration of the ash sample was needed. However, high volcanic ash concentration might contaminate the PA cell which led to the increase of PA signal in background S_b due to the absorption of residual particles on the walls or/and on the windows of the PA cell. Therefore, appropriate volcanic ash concentrations, sufficient for the measurement using red laser and not too high to perturb the background PA signal, are needed in this experiment. Volcanic ash concentrations (black dots in Fig. 6) ranging from 0.5 to 6.5 mg/m^3 were generated in the present work. Once the volcanic ash concentration was stable, the PA signals from the blue, green, and red lasers were sequentially acquired, as shown in Fig. 6 (blue area). The background PA signals due to excitations by blue, green, and red lasers (grey area in Fig. 6) were regularly checked after each measurement.

Figure 7 shows PA signals versus the corresponding volcanic ash mass concentrations of sample

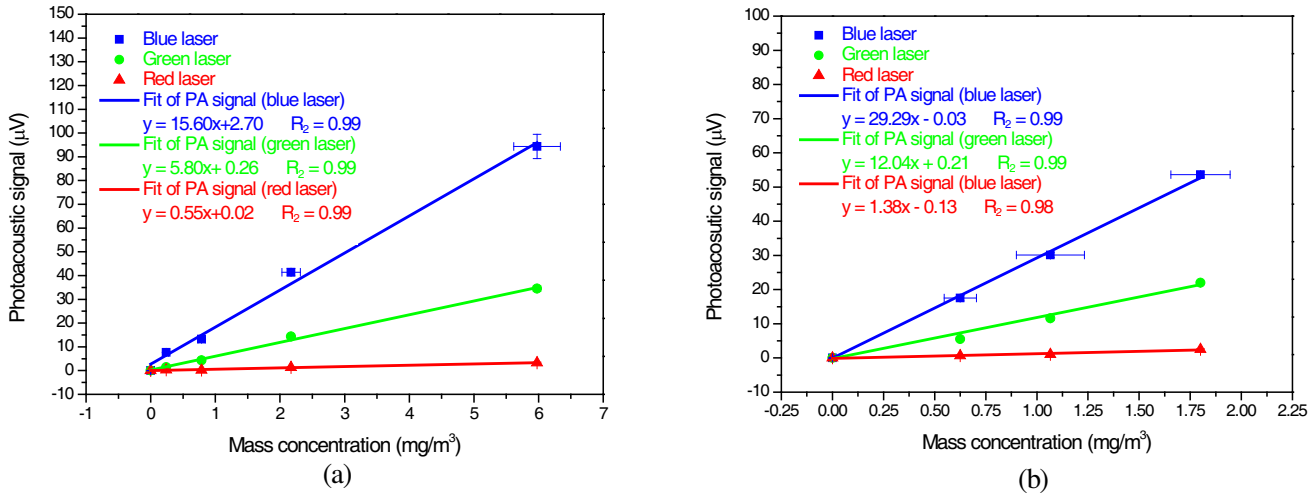

Figure 7. Linear responses of PA signals (from excitation by blue, green and red lasers) to volcanic ash mass concentrations of (a) sample A and (b) sample B.

A (Fig. 7(a)) and sample B (Fig. 7(b)). Fig. 7(a) shows the linear response of PA signals to the mass concentrations of sample A with linear fits ($R^2 = 0.99$) of $y = 15.6x + 2.70$ (for blue laser), $y = 5.80x - 0.26$ (for green laser), $y = 0.55x + 0.02$ (for red laser), respectively. For sample B, Fig. 7(b) shows linear fits of $y = 29.29x - 0.03$ (blue laser), $y = 12.04x + 0.21$ (green laser), and $y = 1.38x - 0.13$ (red laser), with regression coefficients $R^2 = 0.99$, 0.99, and 0.98, respectively.

For calculation of wavelength-dependent mass absorption coefficient (α_{MAC}) of the volcanic ashes, the following equation is used:

$$\alpha_{\mathrm{MAC}} = \frac{S_{\mathrm{slope}}}{P \times M \times C_{\mathrm{cell}}} \tag{7}$$

where S_{slope} is the slope of linear fit of the PA signals to volcanic ash mass concentrations (obtained in Fig. 7). The determined α_{MAC} for sample A and sample B are given in Table 2. The total measurement uncertainties for the determined α_{MAC} are dependent on the uncertainties in the PA signals, fluctuations in volcanic ash concentrations, power measurement accuracy, and uncertainties in the determined cell constant C_{cell}, as shown in Table 2. The measurement uncertainties for samples A and B are 11.47% and 14.50%, respectively, while the measurement uncertainty in the routine filter-based techniques is in the range of 20–30%. The main uncertainty comes from the fluctuations in volcanic ash concentrations. Limits of detection of the used PA spectrophone is evaluated to be $0.42\,\mathrm{Mm}^{-1}$ (444 nm), $1.67\,\mathrm{Mm}^{-1}$ (532 nm), and $7.97\,\mathrm{Mm}^{-1}$ (660 nm) for sample A and $0.53\,\mathrm{Mm}^{-1}$ (444 nm), $1.95\,\mathrm{Mm}^{-1}$ (532 nm), and $10.64\,\mathrm{Mm}^{-1}$ (660 nm) for sample B for 1 s integration time, respectively.

Figure 8 shows a comparison of our measured α_{MAC} with Lima's results [30]. Lima et al. [30] derived the spectral light absorption of volcanic ashes from Eyjafjallajökull by measuring the reflectance of a filter deposited with volcanic ashes using a broadband illuminator from 350 to 2500 nm. The reflected lights from the loaded filters were comparatively analyzed to a blank filter. Lima et al. determined the α_{MAC} for two types of volcanic ashes (fine and mixed states) using the optical reflectance method. The "fine" (red curve) and "mixed" (blue curve) volcanic ashes were collected using filters with pores of 0.4 and 5 μm, respectively. Fig. 8 shows that α_{MAC} of sample A are consistent with α_{MAC} of Lima's fine volcanic ashes [30], while α_{MAC} of sample B are higher than the value from Lima's measurements. The difference might result from their chemical compositions. The main chemical compositions of volcanic ashes are SiO and alkali (such as Al_2O_3, FeO, CaO etc.), and high alkali content leads to high light absorption [32, 33]. Lima et al. showed that different sulfate particles content between the "fine" and "mixed" ash samples result in different absorptions in the UV-visible spectrum [30].

The wavelength-dependent mass absorption coefficient is characterized by the absorption Ångström coefficient (AAC) parameter and can be expressed using a power law equation in the visible spectral

Table 2. Mass absorption coefficients (MAC) of volcanic ashes sample A and B determined with the 3-wavelength PA spectrophone and APS. Measurement uncertainties due to the fluctuations in the PA signals (U-PA), in the light power (U-LP), in the volcanic ash concentrations (U-VA) and uncertainties in the calibrated cell constant C_{cell} (U-C). 1-σ limit of detection (LOD) of 3-wavelength PA spectrophone at 444, 532 and 660 nm determined with sample A and B for 1 s integration time.

Wavelength (nm)	α_{MAC} (m^2/g) sample A	α_{MAC} (m^2/g) sample B	Total uncertainties (%) (A/B)	U-PA (%) (A/B)	U-LP (%)	U-VA (%) (A/B)	U-C (%)	LOD (Sample A) (1σ) (Mm^{-1})	LOD (Sample B) (1σ) (Mm^{-1})
444 nm	0.102 ± 0.011	0.192 ± 0.025	10.37/12.90	3.4/2.4	0.2			0.42	0.53
532 nm	0.055 ± 0.006	0.114 ± 0.015	10.47/13.15	3.7/3.5	0.2	8.9/12	4.1	1.67	1.95
660 nm	0.027 ± 0.004	0.067 ± 0.012	13.58/17.45	9.4/12	2.4			7.97	10.64

region [34, 35]:

$$\alpha_{\text{MAC}} = K \times \lambda^{-\text{AAC}} \tag{8}$$

where K is a constant that includes the PM mass concentration. λ is the wavelength. Carbonaceous particulate matter is considered as one of the main drivers in global warming [36–39]. It can be classified as black carbon (BC) and brown carbon (BrC) [37, 38]. BC is characterized by its strong absorption in the visible. The AAC of BC is commonly considered as around 1–1.3 [39], and the AAC of BrC is in the range of 2–11 which indicates that the light absorption of BrC strongly depends on the wavelength [40].

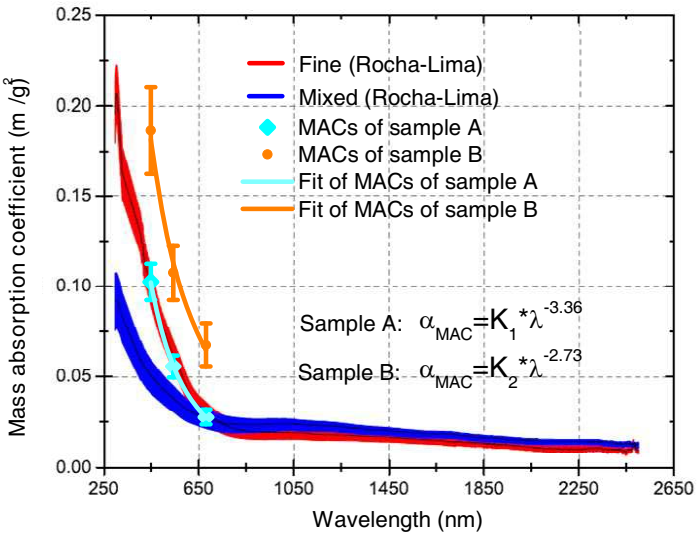

Figure 8. Comparison of the measured mass absorption coefficient with the data from Lima et al. [30] and power equation fit of the MAC of sample A (light blue line) and sample B (orange line). K_1 and K_2 are constant.

In the present work, power equation fits of the α_{MAC} of samples A (light blue line) and B (orange line) versus wavelengths result in AAC $= 3.36 \pm 0.38$ and 2.73 ± 0.39 for samples A and B, respectively. This first demonstration of using PA spectrophone to make filter-free measurement of AAC of volcanic ashes provided higher measurement precision. The determined AAC of the volcanic ash sample brings insight into the chemical composition of volcanic ash sample. According to our experimental results and the previous investigations, the main absorption in the volcanic ashes (Eyjafjallajökull) in the UV-visible spectral region is due to brown carbon combined with sulfate and nitrate.

3.3. Field Measurement of Ambient PM

The 3-wavelength PA spectrophone was deployed to a field campaign to measure ambient PM. The measurement site was located at a central traffic junction in a suburban area of Grenoble (France), located next to an intersection of a circular overpass. This site was generally characterized by high traffic circulation especially at rush time.

A reference instrument aethalometer (Magee scientific, Model AE33) was used to measure the ambient PM with a time resolution of 1 min. PM absorption at 880 nm is defined as a standard measurement of black carbon [41]. Brown carbon is known to have stronger light absorption in the ultraviolet wavelength range than in the near-infrared range [42]. Broadband measurements by the aethalometer at 7 wavelengths (370, 470, 520, 590, 660, 880, and 950 nm) allow for spectral analysis of light absorption from brown carbon and black carbon [41, 42].

In ambient PM measurements, spectral interference from atmospheric gases (in particular NO_2 absorption at the working wavelengths of the PA spectrophone) must be well taken into account. A commonly used method is to perform 2-channel measurements with and without filter (corresponding to without and with aerosol contribution). The difference of the measurements from the 2 channels allows one to remove atmospheric gas absorption and to derive PM absorption.

In our outdoor measurement (unlike our indoor experiments in lab), as the red laser power is too low for sensitive measurement of actual ambient PM of low concentration, only blue and green lasers were used for PM measurements in air. Measurements at two wavelengths (blue and green lasers) took 12 min that were composed of 2 segments of 6 min measurement for each laser. The 2-channel measurements with and without filter for one laser were performed within one segment in 6 min. The PA signals were averaged in 1 min to match the aethalometer time resolution, and three measurement data related to PM absorption were obtained for each laser wavelength every 12 min. The PM absorption coefficient derived from the PA spectrophone is expressed as:

$$\alpha_{\text{abs,aerosol}} = \frac{S_{\text{PA1}} - S_{\text{PA2}}}{P \times M \times C_{\text{cell}}} \tag{9}$$

where S_{PA1} is the measured PA signal due to atmospheric PM and gas absorptions (without filter). S_{PA2} is the measured PA signal due to only gas absorption (with filter). P is the light power. M is the microphone sensitivity, and C_{cell} is the calibrated PA cell constant.

Temperature and humidity of the air sample were monitored at the inlet of the PA cell using a temperature/humidity sensor (Sensirion, SHT10). Time-series measurements of PM absorption coefficients using the PA spectrophone (at 444 and 532 nm) and PM mass concentration measured by the aethalometer (at 470 and 520 nm) are plotted in Figs. 9(a) and 9(b), respectively. The monitored

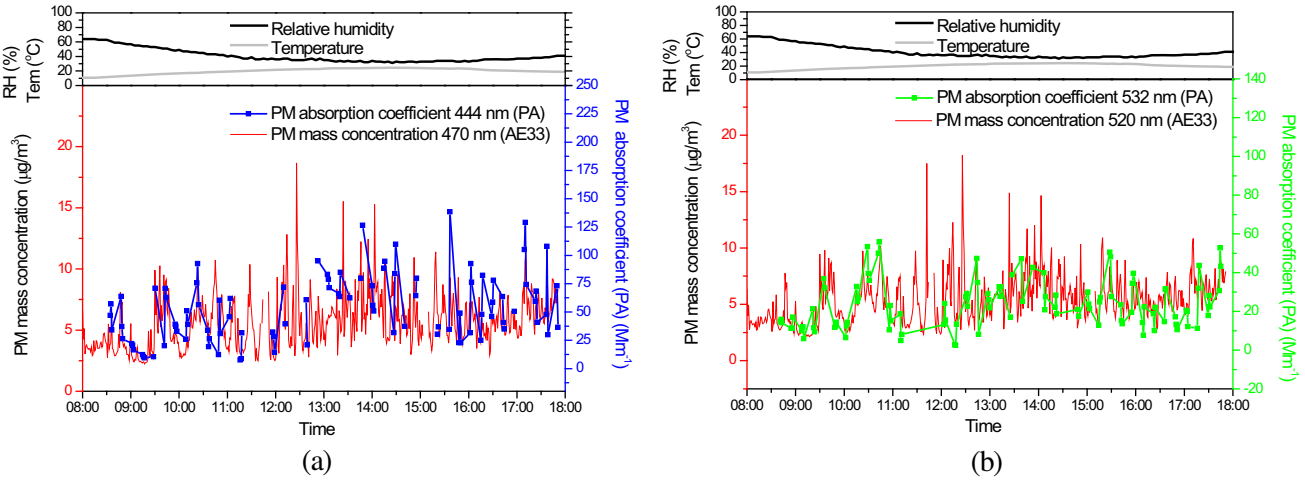

Figure 9. Time-series measurement of ambient PM absorption coefficient (at (a) 444 and (b) 532 nm) by PA spectrophone (blue and green lines), and PM mass concentration (at (a) 470 and (b) 520 nm) by aethalometer (red), and the variation of temperature and relative humidity.

temperature and relative humidity (RH) are associated as well. During the measurement period from 08 h to 18 h, the RH decreased from 64% to 30% for a temperature variation from 10°C to 20°C, no significant RH or temperature impacts on PA signal were observed under this experimental condition.

As the PM absorption coefficient is linearly proportional to the PM mass concentration, the correlation between the measured ambient PM absorption coefficient by PA spectrophone and the ambient PM mass concentration by aethalometer are investigated. Fig. 10(a) shows linear response of ambient PM absorption coefficient measured by PA spectrophone at 444 nm (y) to the ambient PM mass concentrations measured by aethalometer at 470 nm (x) : $y = 8.82x$ with a regression coefficient $R^2 = 0.81$. Fig. 10(b) plots the linear relation of PM absorption coefficient at 532 nm measured by PA spectrophone (y) to the PM mass concentrations at 520 nm from aethalometer (x) : $y = 4.47x$ with a regression coefficient $R^2 = 0.87$. Deduced from the fitted slopes, the field measured ambient PM mass absorption coefficients are $8.82 \pm 4.93\,\mathrm{m^2/g}$ ($\alpha_{\mathrm{MAC},444}$) at 444 nm and $4.47 \pm 1.90\,\mathrm{m^2/g}$ ($\alpha_{\mathrm{MAC},532}$) at 532 nm, respectively.

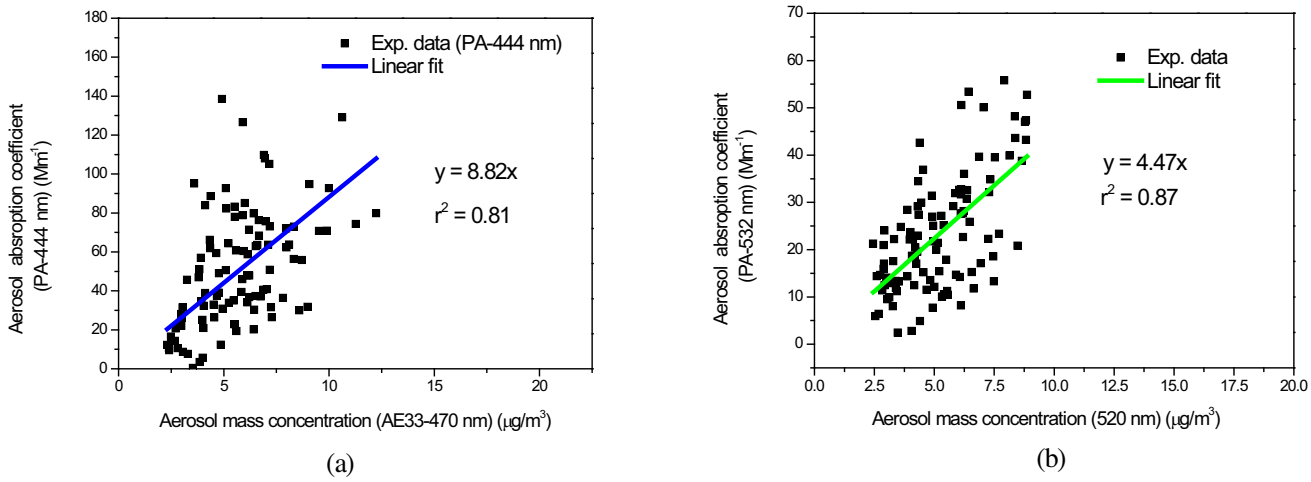

Figure 10. Correlation of ambient PM absorption coefficients measured by PA spectrophone vs. ambient PM mass concentrations measured by aethalometer at (a) 444 nm and (b) 532 nm.

Linke et al. utilized a 3-wavelength PA spectrophone to determine α_{MAC} of ambient PM in a traffic junction which were 10.8 (445 nm), 7.0 (532 nm), 5.9 (660 nm) in a traffic-dominated period. In the period influenced by residential wood burning, α_{MAC} values of 14.8 (445 nm), 8.6 (532 nm), 6.0 (660 nm) were found [24]. Tikhomirov et al. reported α_{MAC} values of $5.5\,\mathrm{m^2/g}$ (532 nm) and $4.5\,\mathrm{m^2/g}$ (694 nm) for ambient PM in a rural area, where the PM results from combustion of carbonaceous fuels and biomass burning [43]. Olson et al. reported α_{MAC} values of 9.3 (470 nm), 8.3 (520 nm), 6.6 (660 nm) $\mathrm{m^2/g}$ for PM from diesel combustion and α_{MAC} values of 3.7 (470 nm), 3.3 (520 nm), 2.7 (660 nm) for wood burning [44]. Our values agree well with the previous investigations in similar environmental sites where ambient PM are realised from traffic emission and wood burning. The reported α_{MAC} of ambient PM determined from similar urban sites are summarized in Table 3.

The absorption Ångström coefficient (AAC) of the ambient PM from 444 to 532 nm can be determined using the following equation:

$$AAC = \frac{\ln\left(\dfrac{\alpha_{\mathrm{MAC},444}}{\alpha_{\mathrm{MAC},532}}\right)}{\ln\left(\dfrac{\lambda_{532}}{\lambda_{444}}\right)} \tag{10}$$

where λ_{444} and λ_{532} are the wavelengths at 444 and 532 nm. An AAC value of 3.63 ± 2.46 for ambient PM is deduced. The uncertainty in AAC is determined using standard uncertainty propagation through Eq. (10). The AAC value of atmospheric PM has a great deal of variability from 1 to 11 due to complex composition in air. Black carbon is commonly considered with AAC of 1 and MAC value at least

Table 3. Mass absorption coefficient of ambient PM at wavelength of 445/470, 520/532 and 660/694 nm. Absorption Ångström coefficient (AAC) at wavelength range of 445/470 to 520/532 nm.

	PM species	α_{MAC} (m^2/g)/λ (nm)			AAC (445–532 nm)*
Linke [24]	Traffic emission	10.80 (445)	7.00 (532)	5.90 (660)	2.42
	Wood burning	14.80 (445)	8.60 (532)	6.00 (660)	3.04
Tikhomirov [43]	Combustion of carbonaceous fuels	/	5.49 (532)	4.46 (694)	/
Olsson [44]	Diesel	9.28 (470)	8.30 (520)	6.61 (660)	1.10
	Wood burning	3.73 (470)	3.34 (520)	2.66 (660)	1.09
Our work	Traffic emission	8.82 (444)	4.47 (532)	/	3.63

*AAC is determined using Eq. (10).

5 m^2/g (550 nm) [37, 39]. The AAC of brown carbon is in the range of 2–11, but with MAC values around 0.4–1.6 m^2/g at 450 nm [40]. Internal mixing ambient PM with BrC coating on BC particles shows enhancement of light absorption, which results in different PM optical properties (AAC and MAC) in the atmosphere [45]. Table 3 shows the determined AAC of different PM using Eq. (10). The AAC value of 3.63 ± 2.46 and MAC values (8.82 m^2/g at 444 nm and 4.47 m^2/g at 532 nm) are well consistent with previous reports and show abundant light absorption particles (BC and BrC) in the atmosphere.

4. CONCLUSIONS AND OUTLOOK

A 3-wavelength PA spectrophone is developed and validated by characterizing volcanic ashes absorption at 444, 532, and 660 nm in lab. The determined AAC values of the volcanic ash samples in the range of 2–3 indicate abundant organic compounds (brown carbon) in volcanic ashes. The PA spectrophone provides high measurement precision: measurement uncertainties of 11.47% and 14.50% for volcanic ash samples A and B compared to the uncertainty of 20–30% in the routine filter-based method. The developed 3-wavelength PA spectrophone is deployed to the measurement of ambient PM in a field campaign. The red laser was not used due to its low light power for sensitive measurement of actual ambient PM of low concentration. The ambient absorption coefficient measured by 3-wavelength PA spectrophone shows a good relation with the measured PM mass concentration by an reference aethalometer.

In the present work, a single PA cell was used for individual measurement at each wavelength, which results in a relatively low temporal resolution (of 12 min). Low time resolution might cause potential error in the measurements of atmospheric PM that is sensitive to environmental conditions such as temperature and relative humidity. The future work will be carried out on the development of an appropriate PA spectrophone capable of simultaneously measuring PM at different wavelengths in order to improve temporal resolution and accuracy of the measurement. Fischer and Smith developed a 4-wavelength PA spectrophone using a single acoustic resonator for simultaneous measurement of PM absorption at 406, 532, 662, and 785 nm, respectively [25]. The quality factor of the resonator is 30 determined from the resonant frequency of 1400 Hz with a resonant frequency FWHM (Full width at half maximum) of 47 Hz. The four diode lasers were modulated at different frequencies (spaced by 2 Hz) within the resonance frequency bandwidth [25]. The frequency space of 2 Hz between different resonant frequencies might be an issue related to cross-talking among these very close modulation frequencies. Liu et al. reported a novel single PA cell containing 3 acoustic resonators for simultaneous multi-component measurement with a frequency space of 110 Hz between different resonant frequencies [46]. In the future, a 3-wavelegnth PA spectrophone based on the novel single PA cell will be developed for accurate simultaneous measurement of PM absorption at 3 wavelengths.

ACKNOWLEDGMENT

This work was funded by the French national research agency (ANR) under the CaPPA (ANR-10-LABX-005) and MABCaM (ANR-16-CE04-0009). The authors thank Lieven Clarisse (CQP, Université Libre de Bruxelles) for providing volcanic ash samples.

REFERENCES

1. Myhre, G., D. Shindell, F. M. Bréon, W. Collins, J. Fuglestvedt, J. Huang, D. Koch, J. F. Lamarque, D. Lee, B. Mendoza, T. Nakajima, A. Robock, G. Stephens, T. Takemura, and H. Zhang, "Anthropogenic and natural radiative forcing," *Climate Change 2013: The Physical Science Basis. Contribution of Working Group I to the Fifth Assessment Report of the Intergovernmental Panel on Climate Change*, 678–698, Cambridge University Press, Cambridge, 2013.
2. Kinne, S., M. Schulz, C. Textor, S. Guibert, Y. Balkanski, S. E. Bauer, T. Berntsen, T. F. Berglen, O. Boucher, M. Chin, W. Collins, F. Dentener, T. Diehl, R. Easter, J. Feichter, D. Fillmore, S. Ghan, P. Ginoux, S. Gong, A. Grini, J. Hendricks, M. Herzog, L. Horowitz, I. Isaksen, T. Iversen, A. KirkevÅg, S. Kloster, D. Koch, J. E. Kristjansson, M. Krol, A. Lauer, J. F. Lamarque, G. Lesins, X. Liu, U. Lohmann, V. Montanaro, G. Myhre, J. E. Penner, G. Pitari, S. Reddy, O. Seland, P. Stier, T. Takemura, and X. Tie, "An AeroCom initial assessment — Optical properties in aerosol component modules of global models," *Atmos. Chem. Phys.*, Vol. 6, 1815–1834, 2006.
3. Loeb, N. G. and W. Su, "Direct aerosol radiative forcing uncertainty based on a radiative perturbation analysis," *J. Climate*, Vol. 23, 5288–5293, 2010.
4. Ajtai, T., Á. Filep, M. Schnaiter, Linke, M. Vragel, Z. Bozóki, G. Szabóa, and T. Leisner, "A novel multi-wavelength photoacoustic spectrometer for the measurement of the UV-vis-NIR spectral absorption coefficient of atmospheric aerosols," *J. Aerosol. Sci.*, Vol. 41, 1020–1029, 2010.
5. Moosmüller, H., R. K. Chakrabarty, and W. P. Arnott, "Aerosol light absorption and its measurement: A review,," *J. Quant. Spectrosc. Rad. Transfer*, Vol. 110, 844–878, 2009.
6. Lack, D. A., H. Moosmüller, G. R. McMeeking, R. K. Chakrabarty, and D. Baumgardner, "Characterizing elemental, equivalent black, and refractory black carbon aerosol particles: A review of techniques, their limitations and uncertainties," *Anal. Bioanal Chem.*, Vol. 406, 99–122, 2014.
7. Kim, K. H., E. Kabir, and S. Kabir, "A review on the human health impact of airborne particulate matter," *Environ. Int.*, Vol. 74, 136–143, 2015.
8. Anderson, J. O., J. G. Thundiyil, and A. Stolbach, "Clearing the air: A review of the effects of particulate matter air pollution on human health," *J. Med. Toxicol.*, Vol. 8, 166–175, 2012.
9. Ram, K. and M. M. Sarin, "Absorption coefficient and site-specific mass absorption efficiency of elemental carbon in aerosols over urban, rural, and high-altitude sites in India," *Environ. Sci. Technol.*, Vol. 43, 8233–8239, 2009.
10. Weingartnera, E., H. Saathoff, M. Schnaiterb, N. Streita, B. Bitnarc, and U. Baltenspergera, "Absorption of light by soot particles: Determination of the absorption coefficient by means of aethalometers," *J. Aerosol Sci.*, Vol. 34, 1445–1463, 2003.
11. Schmid, O., P. Artaxo, W. P. Arnott, D. Chand, L. V. Gatti, G. P. Frank, A. Hoffer, M. Schnaiter, and M. O. Andreae, "Spectral light absorption by ambient aerosols influenced by biomass burning in the Amazon Basin. I: Comparison and field calibration of absorption measurement techniques," *Atmos. Chem. Phys.*, Vol. 6, 3443–3462, 2006.
12. Lack, D. A., E. R. Lovejoy, T. Baynard, A. Pettersson, and A. R. Ravishankara, "Aerosol absorption measurement using photoacoustic spectroscopy: Sensitivity, calibration, and uncertainty developments," *Aerosol Sci. Technol.*, Vol. 40, 697–708, 2006.
13. Thompson, J. E., N. Barta, D. Policarpio, and R. DuVall, "A fixed frequency aerosol albedometer," *Opt. Express*, Vol. 18, 2191–2205, 2008.
14. Onasch, T. B., P. Massoli, P. L. Kebabian, F. B. Hills, F. W. Bacon, and A. Freedman, "Single scattering albedo monitor for airborne particulates," *Aerosol Sci. Tech.*, Vol. 49, 267–279, 2015.

15. Davies, N. W., M. I. Cotterell, C. Fox, K. Szpek, J. M. Haywood, and J. M. Langridge, "On the accuracy of aerosol photoacoustic spectrometer calibrations using absorption by ozone," *Atmos. Meas. Tech.*, Vol. 11, 2313–2324, 2018.
16. Arnott, W. P., H. Moosmüller, C. F. Rogers, T. Jin, and R. Bruch, "Photoacoustic spectrometer for measuring light absorption by aerosol: Instrument description," *Atmos. Environ.*, Vol. 33, 2845–2852, 1999.
17. Sigrist, M. W., *Air Monitoring by Spectroscopic Techniques*, John Wiley and Sons, New York, USA, 1994.
18. Miklós, A. and P. Hess, "Application of acoustic resonators in photoacoustic trace gas analysis and metrology," *Rev. Sci. Instrum.*, Vol. 72, 1937–1955, 2001.
19. Bergstrom, R. W., P. Pilewskie, P. B. Russell, J. Redemann, T. C. Bond, P. K. Quinn, and B. Sierau, "Spectral absorption properties of atmospheric aerosols," *Atmos. Chem. Phys.*, Vol. 7, 5937–5943, 2007.
20. Wiegand, J. R., L. D. Mathews, and G. D. Smith, "A UV-V is photoacoustic spectrophotometer," *Anal. Chem.*, Vol. 86, 6049–6056, 2014.
21. Sharma, N., I. J. Arnold, H. Moosmüller, W. P. Arnott, and C. Mazzoleni, "Photoacoustic and nephelometric spectroscopy of aerosol optical properties with a supercontinuum light source," *Atmos. Meas. Tech.*, Vol. 6, 3501–3513, 2013.
22. Radney, J. G. and C. D. Zangmeister, "Measurement of gas and aerosol phase absorption spectra across the visible and near-IR using supercontinuum photoacoustic spectroscopy," *Anal. Chem.*, Vol. 87, 7356–7363, 2015.
23. Lewis, K., W. P. Arnott, H. Moosmüller, and C. E. Wold, "Strong spectral variation of biomass smoke light absorption and single scattering albedo observed with a novel dual-wavelength photoacoustic instrument," *J. Geophys. Res.*, Vol. 113, D16203, 2008.
24. Linke, C., I. Ibrahim, N. Schleicher, R. Hitzenberger, M. O. Andreae, T. Leisner, and M. Schnaiter, "A novel single-cavity three-wavelength photoacoustic spectrometer for atmospheric aerosol research," *Atmos. Meas. Tech.*, Vol. 9, 533–5346, 2016.
25. Fischer, D. A. and G. D. Smith, "A portable, four-wavelength, single-cell photoacoustic spectrometer for ambient aerosol absorption," *Aerosol Sci. Tech.*, Vol. 52, 393–406, 2018.
26. Fischer, C., M. W. Sigrist, Q. Yu, and M. Seiter, "Photoacoustic monitoring of trace gases by use of a diode-based difference frequency laser source," *Opt. Lett.*, Vol. 26, 1609–1611, 2001.
27. Wang, G., F. Shen, H. Yi, P. Hubert, A. Deguine, D. Petitprez, R. Maamary, P. Augustin, M. Fourmentin, E. Fertein, M. W. Sigrist, T.-N. Ba, and W. Chen, "Laser absorption spectroscopy applied to monitoring of short-lived climate pollutants (SLCPs)," *J. Mol. Spectrosc.*, Vol. 348, 142–151, 2018.
28. Arnott, W. P., H. Moosmüller, and J. W. Walker, "Nitrogen dioxide and kerosene-flame soot calibration of photoacoustic instruments for measurement of light absorption by aerosols," *Rev. Sci. Instrum.*, Vol. 71, 4545–4552, 2000.
29. Voigt, S., J. Orphal, and J. P. Burrow, "The temperature and pressure dependence of the absorption cross-sections of NO_2 in the 250–800 nm region measured by Fourier-transform spectroscopy," *J. Photochem. Photobiol. A: Chem.*, Vol. 149, 1–7, 2002.
30. Lima, A. R., J. V. Martins,, L. A. Remer, N. A. Krotkov, M. H. Tabacniks, Y. B. Ami, and P. Artaxo, "Optical microphysical and compositional properties of the Eyjafjallajökull volcanic ash," *Atmos. Chem. Phys.*, Vol. 14, 10649–10661, 2014.
31. Dragosics, M., O. Meinander, T. Jónsdóttír, T. Dürig, G. D. Leeuw, F. Pálsson, P. D. Waldhauserová, and T. Thorsteinsson, "Insulation effects of Icelandic dust and volcanic ash on snow and ice," *Arab J. Geosci.*, Vol. 9, 126, 2016.
32. Vogel, A., S. Diplas, A. J. Durant, A. S. Azar, M. F. Sunding, W. I. Rose, A. Sytchkova, C. Bonadonna, K. Krüger, and A. Stohl, "Reference data set of volcanic ash physicochemical and optical properties," *J. Geophys. Res. Atmos.*, Vol. 122, 9485–9514, 2016.

33. Schumann, U., B. Weinzierl, O. Reitebuch, H. Schlager, A. Minikin, C. Forster, R. Baumann, T. Sailer, K. Graf, H. Mannstein, C. Voigt, S. Rahm, R. Simmet, M. Scheibe, M. Lichtenstern, P. Stock, H. Rüba, D. Schäuble, A. Tafferner, M. Rautenhaus, T. Gerz, H. Ziereis, M. Krautstrunk, C. Mallaun, J.-F. Gayet, K. Lieke, K. Kandler, M. Ebert, S. Weinbruch, A. Stohl, J. Gasteiger, S. Groß, V. Freudenthaler, M. Wiegner, A. Ansmann, M. Tesche, H. Olafsson, and K. Sturm, "Airborne observations of the Eyjafjalla volcano ash cloud over Europe during air space closure in April and May 2010," *Atmos. Chem. Phys.*, Vol. 11, 2245–2279, 2011.
34. Alexander, D. and A. Kokhanovsky, *Light Absorption and Scattering by Particles in the Atmosphere*, Praxis Publishing Ltd., Chichester, UK, 2008.
35. Andreae, M. O. and A. Gelencsér, "Black carbon or brown carbon? The nature of light-absorbing carbonaceous aerosols," *Atmos. Chem. Phys.*, Vol. 6, 3131–3148, 2006.
36. Bond, T. C. and R. W. Bergstrom, "Light absorption by carbonaceous particles: An investigative review," *Aerosol Sci. Tech.*, Vol. 40, 27–67, 2006.
37. Bond, T. C., S. J. Doherty, D. W. Fahey, P. M. Forster, J. Berntsen, T. B. DeAngelo, M. G. Flanner, S. Ghan, B. Kärcher, D. Koch, S. Kinne, Y. Kondo, P. K. Quinn, M. C. Sarofim, M. G. Schultz, M. Schulz, C. Venkataraman, H. Zhang, S. Zhang, N. Bellouin, S. K. Guttikunda, P. K. Hopke, M. Z. Jacobson, J. W. Kaiser, Z. Klimont, U. Lohmann, J. P. Schwarz, D. Shindell, and T. Storelvmo, "Bounding the role of black carbon in the climate system: A scientific assessment," *J. Geophys. Res. Atmos.*, Vol. 118, 5380–5552, 2013.
38. Laskin, A., J. Laskin, and S. A. Nizkorodov, "Chemistry of atmospheric brown carbon," *Chem. Rev.*, Vol. 115, 4335–4382, 2015.
39. Lack, D. A. and J. M. Langridge, "On the attribution of black and brown carbon light absorption using the Ångström exponent," *Atmos. Chem. Phys.*, Vol. 13, 10535–10543, 2013.
40. Feng, Y., V. Ramanathan, and V. R. Kotamarthi, "Brown carbon: A significant atmospheric absorber of solar radiation?," *Atmos. Chem. Phys.*, Vol. 13, 8607–8621, 2013.
41. Sandradewi, J., A. S. H. Prévôt, S. Szidat, N. Perron, M. R. Alfarra, V. A. Lanz, E. Weingartner, and U. Baltensperger, "Using aerosol light absorption measurements for the quantitative determination of wood burning and traffic emission contributions to particulate matter," *Environ. Sci. Technol.*, Vol. 42, 3316–3323, 2008.
42. Drinovec, L., G. Močnik, P. Zotter, A. S. H. Prévôt, C. Ruckstuhl, E. Coz, M. Rupakheti, J. Sciare, T. Müller, A. Wiedensohler, and A. D. A. Hansen, "The "dual-spot" Aethalometer: An improved measurement of aerosol black carbon with real-time loading compensation," *Atmos. Meas. Tech.*, Vol. 8, 1965–1979, 2015.
43. Tikhomirov, A. T., K. F. Firsov, V. K. Kozlov, M. P. Panchenko, Y. P. Ponomarev, and B. T. Tikhomirov, "Investigation of spectral dependence of shortwave radiation absorption by ambient aerosol using time-resolved photoacoustic technique," *Opt. Eng.*, Vol. 44, 071203, 2005.
44. Olson, M. R., M. V. Garcia, M. A. Robinson, P. V. Rooy, M. A. Dietenberger, M. Bergin, and J. J. Schauer, "Investigation of black and brown carbon multiple wavelength dependent light absorption from biomass and fossil fuel source emissions," *J. Geophys. Res. Atmos.*, Vol. 120, 6682–6697, 2015.
45. Devi, J. J., M. H. Bergin, M. Mckenzie, J. J. Schauer, and R. J. Weber, "Contribution of particulate brown carbon to light absorption in the rural and urban Southeast US," *Atmos. Environ.*, Vol. 136, 95–104, 2016.
46. Liu, K., J. Mei, W. Zhang, W. Chen, and X. Gao, "Multi-resonator photoacoustic spectroscopy," *Sensor. Actuat. B-Chem.*, Vol. 251, 632–636, 2017.